electronics

Article

Performance Evaluation of Solar-PV-Based Non-Isolated Switched-Inductor and Switched-Capacitor High-Step-Up Cuk Converter

Neeraj Priyadarshi [1], Mahajan Sagar Bhaskar [2], Farooque Azam [3], Mayank Singh [4], Dheeraj Kumar Dhaked [4], Ibrahim B. M. Taha [5] and Mohamed G. Hussien [6,*]

[1] Department of Electrical Engineering, JIS College of Engineering, Kolkata 741235, India; neerajrjd@gmail.com
[2] Renewable Energy Lab, College of Engineering, Prince Sultan University, Riyadh 11586, Saudi Arabia; sagar25.mahajan@gmail.com
[3] School of Computer Science and Engineering, REVA University, Bangalore 560064, India; farooque53786@gmail.com
[4] Department of Electrical Engineering, Rajasthan Technical University, Kota 324010, India; singhmayank1194@gmail.com (M.S.); ddhakar9@gmail.com (D.K.D.)
[5] Electrical Engineering Department, College of Engineering, Taif University, P.O. Box 11099, Taif 21944, Saudi Arabia; i.taha@tu.edu.sa
[6] Electrical Power and Machines Engineering Department, Faculty of Engineering, Tanta University, Tanta 31527, Egypt
* Correspondence: mohamed.hussien3@f-eng.tanta.edu.eg

Citation: Priyadarshi, N.; Bhaskar, M.S.; Azam, F.; Singh, M.; Dhaked, D.K.; Taha, I.B.M.; Hussien, M.G. Performance Evaluation of Solar-PV-Based Non-Isolated Switched-Inductor and Switched-Capacitor High-Step-Up Cuk Converter. *Electronics* **2022**, *11*, 1381. https://doi.org/10.3390/electronics11091381

Academic Editor: Noel Rodriguez

Received: 23 February 2022
Accepted: 22 April 2022
Published: 26 April 2022

Abstract: Solar photovoltaic (PV) is the most promising renewable energy source available on Earth. Three topologies based on a switched-inductor capacitor and non-isolated high-step-up Cuk converter have been proposed for solar PV. These topologies of the Cuk converter have higher boosting ability than conventional Cuk and boost converters and can reduce the voltage stress of the main switch. A small voltage rating and on-state resistance can give higher efficiency of the converter. The voltage boosting ability of all three topologies was compared to each other and with a conventional Cuk converter. The boosting capability of the third converter was 11 times at 0.75 duty cycle with a solar PV source. These converters do not use a coupled inductor and transformer, which leads to less volume, reducing coupling/core saturation loss, and thus the cost of the converter. A solar PV system of 12 volts was used for boosting with these converters for analysis of the feasibility of use with renewables. The three topologies of the switched-inductor and switched-capacitor (SLSC) Cuk converter were designed and simulated in MATLAB/Simulink to evaluate their effectiveness.

Keywords: Cuk converter; voltage boosting; solar PV; DC-DC converter; switched-capacitor; switched-inductor

1. Introduction

World energy demand is growing linearly while fossil fuel supplies, such as petroleum, coal, and natural gases may be depleted in the near future. The major issues with fossil-fuel-based energy generation are greenhouse gas emissions and carbon footprint. The growing energy demand cannot be met solely through sources such as thermal, hydro, nuclear, etc. As a result, it is essential to use alternative energy or renewable energy sources which are abundant and freely available to overcome the global energy crisis and meet future energy demands. Solar energy is of the utmost importance among renewable energy sources because it is pollution-free and inexhaustible [1]. Its use is becoming increasingly common these days because non-renewable energy can harm and affect the environment and nature. The key advantages of photovoltaic (PV) applications are that they are clean, emission free, and have a high level of reliability [2]. PV cells are used to extract a usable electrical form of energy from solar energy. Renewable energy sources, such as solar, give low voltage output that needs to be boosted to higher functional levels [3,4]. The primary consideration in renewable applications is how to achieve high voltage gain while maintaining more efficiency during voltage boosting. By 2040, PV will be the most crucial source of power generation among all renewable energy candidates [5].

DC to DC conversion is now employed in numerous sectors and applications, including renewable sources, EV charging stations, uninterrupted power supply, electric trains, and others [6]. Low DC output voltages are standard in PV and fuel cells, requiring high voltage gain DC-DC converters to connect them to the grid [7–10]. The converter must have a steady input current to obtain extreme power from the solar panels. More voltage gain from an uninterrupted input supply current determines the suitability of converters for renewable energy applications [11,12]. A novel continuous step/down and step switched-capacitor (SC)-based DC-DC converter has been suggested to have many advantages, such as lower voltage stress for capacitors and higher voltage gain than formerly proposed DC-DC converters [13]. In another paper, a new high voltage amplification DC-DC converter with a coupled inductor and voltage multiplier (VM) cell is described. Converter behavior is relied on for charging capacitors using a single MOSFET switch and adding sources in series from the source to the load [14]. A novel non-solidified DC-DC Cuk and boost converter assembly with high voltage amplification is proposed. The presented topology consists of a boost and a Cuk converter with a low power voltage ripple and high voltage gain in comparison to the conventional boost and Cuk converter [15]. In [16], an effective method based on the Harris Hawks optimization algorithm (HHO) to select the optimal capacity, number, and location of solar-based DGs to reduce active power loss and voltage deviation is used. The authors of [17] describe the improvement in an effective non-isolated switched-capacitor coupled-inductor boost-converter structure. Switched capacitors decrease the voltage stress of power semiconductor switches, reduce device conduction losses, and enable the use of low on-resistance switches. In addition, passive clamp circuits can be used to achieve zero current to turn diodes and solid-state power switches on and off naturally [17]. A high static gain DC-DC converter with a single switch for efficient photovoltaic (PV)-based grid applications is proposed in [18]. This proposed topology is derived from SEPIC (single-ended primary inductor converter) by presenting a voltage doubler circuit to reduce voltage stress across semiconductor devices and provide high voltage gain [18].

This research study considers the requirement by renewable energy applications for high voltage gain with uninterrupted input supply current using a DC-DC converter. A solar PV system is used to generate three different topologies derived from a Cuk converter. The solar PV renewable source can reduce the effect of environmental deteriorating agents produced by conventional power generating stations. A conventional Cuk converter is modified to create three different topologies based on a switched-inductor and a switched-capacitor (SLSC). The improvement implemented involves putting an SC unit in the place of the capacitor, and placing an SL unit in the position of the inductors. The proposed converter produces less noise, has a high transient response, and has minimal electromagnetic interference. Climate issues lead to the degradation of photovoltaic panels; temperature is the most degrading factor for solar panels as they are exposed to sunlight [19–21]. This issue must be considered in countries such as India, Egypt, and Saudi Arabia; however, manufacturers' statements are often given for lower temperatures and different conditions than the real-world conditions experienced. This paper does not consider the durability of panels.

The voltage boosting provided by these converters is negative to positive. The objectives of the study are as follows:

1. To introduce the basics of the Cuk converter and different derived topologies based on switched-inductor and switched-capacitor (SLSC) and a high-gain step-up Cuk converter.
2. To study a PV system with a DC-DC converter.

3. To implement the Simulink model of the three converters considered with solar PV on the MATLAB platform.
4. To study the behavior of the converter and analyze its characteristics.
5. To compare the boosting ability of a conventional boost converter with the discussed topologies.

2. Photovoltaic Generator Mathematical Modeling

The PV array parameters depend on several environmental factors [22,23]. However, designers have only used parameters for standard test conditions (STC). Accurate PV modeling is essential to implement maximum power point tracking (MPPT) algorithms, and other controlling methods [24,25]. Hence, this research employed a modified uni-diode modeling (MUDM)-based PV system, which provides more straightforward implementation and reliable operation for power generation under varying atmospheric conditions. Compared to the ideal single diode model (ISDM) and the single diode model (SDM), modified uni-diode modeling (MUDM) enables more straightforward implementation. It also provides a more accurate response and easier modeling as ISDM and SDM do not provide precise I–V nature under the maximum power point (MPP) region and require more parameters for estimation, respectively [26].

The I–V curve of a PV module having N_{SRK} cells connected in series (Figure 1) can be derived mathematically as:

$$I_{PHG} = I_{PHN} - I_{SAT}\left[e^{\frac{Q_E(V_{PHG}+I_{PHG}R_{SRK}N_{SRK})}{N_{SRK}K_B T_B A_S}} - 1\right] - \frac{V_{PHG} + I_{PHG}R_{SRK}N_{SRK}}{N_{SRK}R_{Parallel}} \quad (1)$$

where, I_{PHG} is PV the output current, I_{PHN} is the photon current, I_{SAT} is the saturation current R_{SRK}, $R_{Parallel}$ are the series and parallel resistor, A_S is the diode ideality factor, Q_E is the electronic charge, K_B is the Boltzmann constant, T_B is the module temperature, and N_{SRK} is PV cells connected in series.

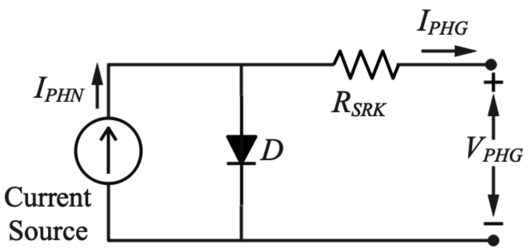

Figure 1. PV cell model.

Mathematically, the I–V relation of the single diode model of a PV system can be expressed by putting R_{SRK} = 0 in Equation (1) as:

$$I_{PHG} = I_{PHN} - I_{SAT}\left[e^{\frac{Q_E(V_{PHG}+I_{PHG}R_{SRK}N_{SRK})}{N_{SRK}K_B T_B A_S}} - 1\right] \quad (2)$$

I_{PHG}, I_{SAT} and I_{SAT} can be evaluated using the below relations as:

$$I_{PHG} = G_{IR}(I_{short} + \alpha_{CT}\Delta T_B) \quad (3)$$

where, G_{IR} is the solar insolation (W/m^2), I_{short} is the short-circuited current at standard test condition, ΔT_B is the temperature difference, and α_{CT} is the coefficient of current temperature. Moreover, I_{short} can be evaluated mathematically as:

$$V_{open}(G_{IR}, T_B) - V_{open}(G_{IR}, T_{STC}) = -|\beta_{VT}|\Delta T_B \quad (4)$$

where, $V_{open}(G_{IR}, T_B)$ is the open-circuited voltage at temperature T_B, $V_{open}(G_{IR}, T_{STC})$ is the open-circuited voltage at T_{STC}, and $|\beta_{VT}|$ is the absolute value of the coefficient of the voltage temperature.

Putting I_{PHG} = 0, V_{open} can be evaluated as:

$$V_{open} = \frac{N_{SRK} K_B T_B A_S}{Q_E} \ln\left(\frac{I_{PHG}}{I_{SAT}} + 1\right) \tag{5}$$

Hence, $V_{open}(G_{IR}, T_B)$ and $V_{open}(G_{IR}, T_{STC})$ shall be evaluated through Equation (5) and refreshing Equation (4) as:

$$\frac{N_{SRK} K_B A_S}{Q_E}\left[T_B \ln\left(\frac{G_{IR}(I_{short} + \alpha_{CT}\Delta T_B)}{I_{short}} + 1\right) - T_{STC}\left(\frac{G_{IR} I_{short}}{I_{RS}} + 1\right)\right] = -|\beta_{VT}|\Delta T_B \tag{6}$$

Moreover, I_{SAT} can be evaluated by the following expressions as:

$$I_{SAT} = \frac{e^{\left(\frac{|\beta_{VT}|\Delta T_B Q_E}{N_{SRK} K_B T_B A_S}\right)} G_{IR}(I_{short} + \alpha_{CT}\Delta T_B)}{\left(\frac{G_{IR} I_{short}}{I_{RS}} + 1\right)^{\frac{T_{STC}}{T_B}} - e^{\left(\frac{|\beta_{VT}|\Delta T_B}{N_{SRK} K_B T_B A_S}\right)}} \tag{7}$$

where, I_{RS} is the reverse saturation current at standard test condition.

$$I_{RS} = \frac{I_{short}}{e^{\left(\frac{Q_E V_{open}}{N_{SRK} K_B T_{STC} A_S}\right)} - 1} \tag{8}$$

Moreover, V_{max} and I_{max} under MPP can be correlated mathematically as:

$$I_{max} = I_{short} - I_{RS}\left[e^{\left(\frac{Q_E V_{max}}{N_{SRK} K_B T_{STC} A_S}\right)} - 1\right] \tag{9}$$

From Equations (8) and (9),

$$\frac{I_{max}}{I_{short}} = e^{\left(\frac{Q_E V_{max}}{N_{SRK} K_B T_{STC} A_S}\right)} - \left(\frac{I_{short} - I_{max}}{I_{short}}\right) e^{\left(\frac{Q_E V_{open}}{N_{SRK} K_B T_{STC} A_S}\right)} \tag{10}$$

3. Hybrid Fuzzy-Logic Sliding Mode Control Based MPPT

In this study, a hybrid fuzzy-logic sliding-mode control (HFLC-SMC)-based MPPT controller was employed in which the fuzzy logic control provides production of V_{Ref} which assimilates with MPP. The entire block diagram is presented in Figure 2. SMC delivers tracking of V_{Ref} produced by the FLC controller using proper adjustment of the duty ratio of the Cuk-SEPIC converter, which results in the generation of zero difference of V_{PV} and V_{Ref}. The fuzzy-logic controller provides accurate responses and does not require any mathematical analysis.

The membership function of error and change in error can be expressed mathematically as:

$$E_{error}(P) = \frac{P_{PVG}(P_k) - P_{PVG}(P_k - 1)}{V_{PVG}(P_k) - V_{PVG}(P_k - 1)} \tag{11}$$

$$dE_{error}(P) = E_{error}(P_k) - E_{error}(P_k - 1) \tag{12}$$

where, $P_{PVG}(P_k)$ is the instantaneous PV power, $V_{PVG}(P_k)$ is the output PV voltage, P_k is the sampling period.

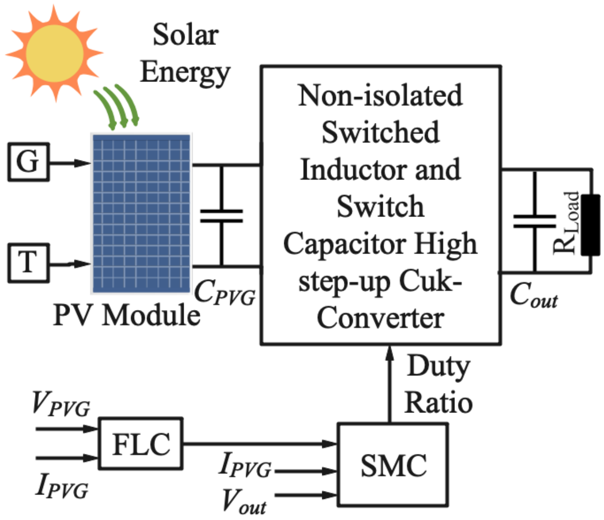

Figure 2. Hybrid FLC-SMC-based MPPT-controlled PV System.

The fuzzy logic output V_{Ref} can be processed using a sliding mode controller and imposed to the Cuk-SEPIC converter. Considering the reference voltage of the PV module V_{Ref} and the output PV voltage V_{PVG} as controlling parameters of SMC, the sliding area can be expressed mathematically as:

$$S_{Area} = \left(K + \frac{d}{dt}\right) E_{error}^{R-1} \tag{13}$$

where, R is the relative degree.

$$E_{error} = Error = V_{PVG} - V_{Ref} \tag{14}$$

$$\dot{Y} = \dot{V}_{PVG} = \frac{I_{PVG}}{C_{PVG}} - \frac{I_{LK}}{C_{PVG}} \tag{15}$$

$$\ddot{Y}_K = \frac{1}{C_{PVG}} \acute{I}_{PVG} - \frac{1}{C_{PVG}} \left[\frac{1}{L_K} V_{PVG} - \frac{1}{L_K}(1 - d_K)\right] V_{out} \tag{16}$$

Put $R = 2$ in Equation (13),

$$S_{Area} = \left(K + \frac{d}{dt}\right) E_{error} = KE_{error} + = \dot{E}_{error} \tag{17}$$

$$\dot{S}_{Area} = \dot{Y}_K - Y_{Ref} = \frac{I_{PVG}}{C_{PVG}} - \frac{I_{LK}}{C_{PVG}} \tag{18}$$

Assuming $\ddot{Y}_K = 0$,

$$\ddot{E}_{error} = \ddot{Y}_K \text{ and } \dot{S}_{Area} = K\dot{V}_{PVG} + \frac{1}{C_{PVG}} \acute{I}_{PVG} \left[\frac{1}{L_K} V_{PVG} - \frac{1}{L_K}(1 - d_K)\right] V_{out} \tag{19}$$

where, K is constant considering the Lyapunov stability function

$$\dot{S}_{Area} = -\lambda Sign(S_{Area}) \tag{20}$$

where, λ is constant. Using Equations (19) and (20),

$$-\lambda Sign(S_{Area}) = K\dot{V}_{PVG} + \frac{1}{C_{PVG}} \acute{I}_{PVG} - \left[\frac{1}{L_K} V_{PVG} - \frac{1}{L_K}(1 - d_K)\right] V_{out} \tag{21}$$

And d_K, the duty ratio, can be evaluated as:

$$d_K = \left[\lambda Sign(S_{Area}) + KV\dot{_{PVG}} + \frac{1}{C_{PVG}}\left(\acute{I}_{PVG} - \frac{1}{L_K}(1-d_K)\right)\right]\frac{L_K C_{PVG}}{Vout} \quad (22)$$

4. Topologies of the CUK Converter

Figure 3 depicts the primary circuit of a conventional Cuk converter. The Cuk converter is utilised for power factor correction applications and has two inductors and two capacitors, which means it has fewer switching losses. The Cuk converter delivers more or less output voltage than the supply voltage with reversed polarity. The inductor L_1 acts as a filter, and the C_1 capacitor decides the extent of energy transfer to the inductor L_1. The load side inductor and capacitor are responsible for extra circuit requirements with less noise, high transient response, and minimised electromagnetic interference. A Cuk converter is a DC-to-DC converter with a negative capacitive output which is like a buck-boost converter. The difference is that the Cuk converter uses a capacitor instead of an inductor for power transfer and energy storage [27]. The input voltage polarity is reversed for the output voltage of the Cuk converter. If linked properly, this converter generates free ripple output that can be useful for various applications [28]. Different circuit topologies of the converter are introduced depending on the Cuk converters in [29]. The effectiveness of the redesigned Cuk converter has been greatly enhanced. This converter is recommended for the excellent bidirectional operation to manage current and voltage [30].

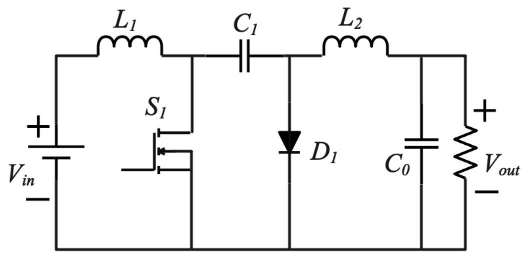

Figure 3. Basic CUK converter.

Within closed-loop systems and fuzzy-logic controllers, several control strategies, e.g., sliding-mode control and traditional proportional-integral (PI) are used to adjust the output voltage [31]. High temperatures affect solar power generation, which is not considered in this study. This study mainly aims to study different topologies of the Cuk converter. This converter is employed in the installation of BLDC motor drives and in PWM.

4.1. Topology-1

This topology is obtained by connecting a switched-inductor (SL) unit with the input side inductor and a switched-capacitor (SC) unit to transfer the energy capacitor. The power circuit schematic of this converter is depicted in Figure 4. Compared to the conventional Cuk prototype, the suggested circuit includes one capacitor, one inductor, and four diodes.

Figure 5a shows the current directions when the switch is turned on (conducting). Through diodes D_1 and D_2, and switch S_1, source voltage V_{in} charges inductors L_1 and L_2 in parallel. During this mode, reversed biased diodes are diodes D_2, D_4, and D_5 and inductor L_3 charged by input voltage through switch, capacitor C_1 and C_2. As both L_1 and L_2 inductors are the same, so the current flowing through them is the same. Figure 5b shows the current direction when the switch is turned off (not conducting). Parallel connected capacitors C_1 and C_2 are charged by the series connection of inductor L_1 and L_2 and input voltage V_{in}. Similarly, the energy discharge by inductor L_3 also charges the capacitors C_1 and C_2 and provides power to load R. During this mode, reverse biased diodes are diodes D_1 and D_3.

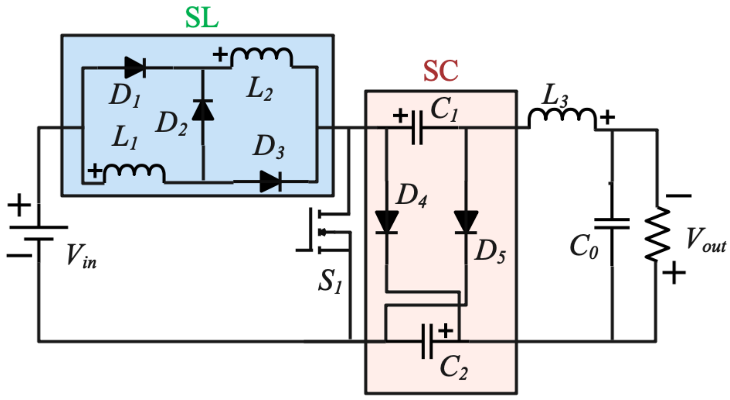

Figure 4. Topology 1: Power circuit of type-1 switched-inductor-switched-capacitor (SLSC) Cuk converter.

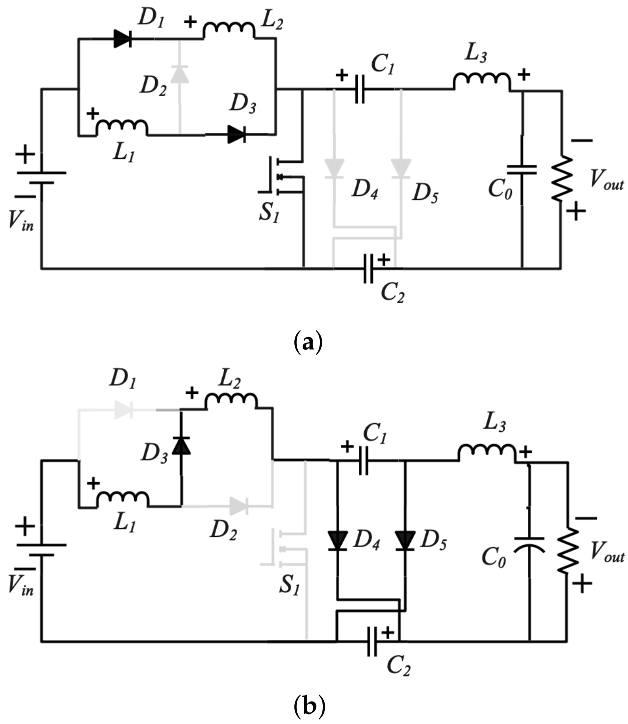

Figure 5. Topology 1: Operating mode of SLSC CUK converter (**a**) ON Mode (**b**) OFF Mode.

Design Analysis of Topology-1

A steady-state analysis of the suggested topology 1 is presented by considering the components are ideal. The source supplies pure DC input voltage V_{in}, and capacitors have a ripple-free voltage. When the switch S_1 is turned ON, the voltages for the inductors are given as:

$$V_{L1} = V_{L2} = V_{in} \tag{23}$$

$$V_{L3} = 2V_C - V_{out} \tag{24}$$

where, $V_C = V_{C1} = V_{C2}$. When switch S_1 is turned off the voltages for inductors are given as:

$$V_{L1} = V_{L2} = \frac{V_{in} - V_C}{2} \tag{25}$$

$$V_{L3} = V_C - V_{out} \tag{26}$$

Applying the volt-second method:

$$V_{in}D + \frac{V_{in} - V_C}{2}(1 - D) = 0 \tag{27}$$

$$(2V_C - V_{out})D + (V_C - V_{out})(1 - D) = 0 \tag{28}$$

The voltage gain is given by,

$$G = \frac{V_{out}}{V_{in}} = \frac{I_{in}}{I_{out}} = \frac{(1 + D)^2}{1 - D} \tag{29}$$

The expression of voltage across switch, capacitors C_1, C_2, and reverse voltage across diodes ($D_1 - D_5$) are given in Table 1.

Table 1. Equations of voltages for type-1 SLSC CUK converter.

Parameters	Expression
Capacitors C_1 and C_2	$\frac{1+D}{1-D}V_{in}$
Switch S_1	$\frac{1+D}{1-D}V_{in}$
Diodes D_1 and D_3	$\frac{D}{1-D}V_{in}$
Diodes D_2	V_{in}
Diodes D_4 and D_5	$\frac{1+D}{1-D}V_{in}$

4.2. Topology-2

This topology is obtained by connecting a switched-inductor (SL) unit with the output side inductor and a switched-capacitor (SC) unit to transfer the energy capacitor. The power circuit of this converter is depicted in Figure 6. Compared to the conventional Cuk prototype, the suggested circuit includes one capacitor, one inductor, and four diodes.

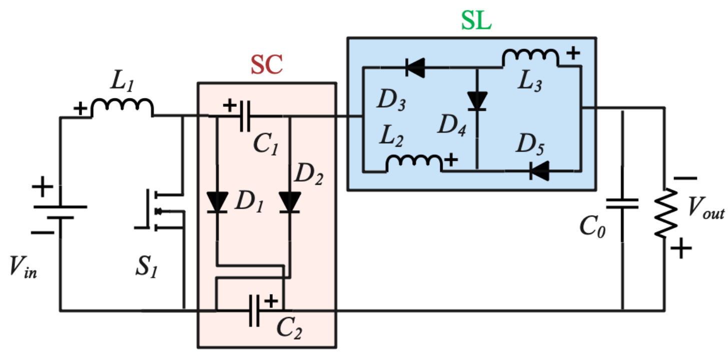

Figure 6. Topology 2: Power circuit of type-2 switched-inductor-switched-capacitor (SLSC) Cuk converter.

Figure 7a shows the equivalent circuit when the switch is turned ON (conducting). The inductor L_1 is charged by source voltage V_{in} through switch S_1. Parallel connected inductors L_2 and inductor L_3 are charged through the switch, diodes D_3 and D_5 by capacitors C_1, C_2 and source voltage V_{in}. As inductors L_2 and L_3 are the same, the current flowing through them is also the same. During this mode, reversed biased diodes are diode D_1, D_2 and D_4. Figure 7b shows the equivalent circuit when the switch is turned OFF (not conducting). Inductors L_1 and source voltage V_{in} charge parallel-connected capacitors C_1 and C_2. Similarly, energy discharge by inductors L_2 and L_3 also charges the capacitors C_1

and C_2 and supplies power to load. During this mode, reversed biased diodes are diodes D_3 and D_5.

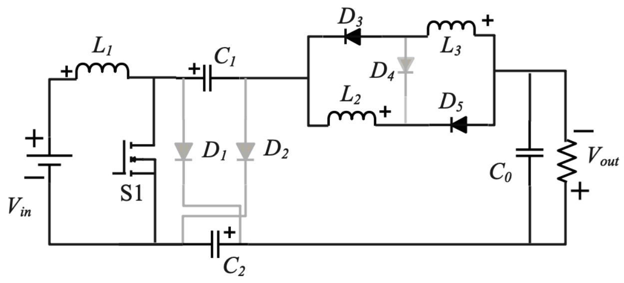

(**a**)

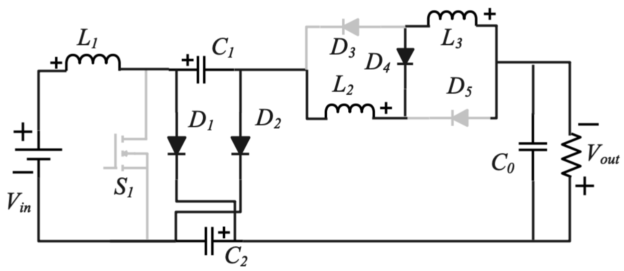

(**b**)

Figure 7. Topology 2: Operating mode of SLSC CUK converter (**a**) ON Mode (**b**) OFF Mode.

Design Analysis of Topology-2

When the switch S_1 is turned ON, the voltages for the inductors are given as:

$$V_{L1} = V_{in} \tag{30}$$

$$V_{L2} = V_{L3} = 2V_C - V_{out} \tag{31}$$

where, $V_C = V_{C1} = V_{C2}$. When switch S_1 is turned off the voltages for the inductors are given as:

$$V_{L1} = V_{in} - V_C \tag{32}$$

$$V_{L2} = V_{L3} = \frac{V_C - V_{out}}{2} \tag{33}$$

Applying the volt-second method:

$$V_{in}D + (V_{in} - V_C)(1 - D) = 0 \tag{34}$$

$$(2V_C - V_{out})D + (\frac{V_C - V_{out}}{2})(1 - D) = 0 \tag{35}$$

The voltage gain is given by,

$$G = \frac{V_{out}}{V_{in}} = \frac{I_{in}}{I_{out}} = \frac{(1 + 3D)}{(1 + D)(1 - D)} \tag{36}$$

The expression of voltage across switch, capacitor C_1, capacitor C_2, and reverse voltage across diodes $(D_1 - D_5)$ are given in Table 2.

Table 2. Equations of voltages for type-2 SLSC CUK converter.

Parameters	Expression
Capacitors C_1 and C_2	$\frac{1}{1-D}V_{in}$
Switch S_1	$\frac{1}{1-D}V_{in}$
Diodes D_1 and D_2	$\frac{1}{1-D}V_{in}$
Diodes D_3 and D_5	$\frac{D}{(1+D)(1-D)}V_{in}$
Diodes D_4	$\frac{1}{1+D}V_{in}$

4.3. Topology-3

This topology is obtained by connecting an SL unit in place of both the input side and the output side inductor and an SC unit in place of the transferring energy capacitor. The power circuit for this converter is depicted in Figure 8. Compared to the conventional Cuk prototype, the suggested circuit includes two capacitors, two inductors and seven diodes.

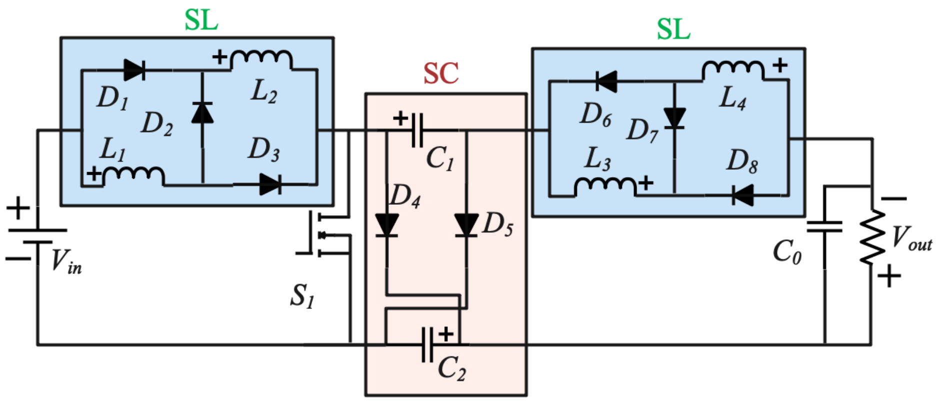

Figure 8. Topology 3: Power circuit of type-2 switched-inductor-switched-capacitor (SLSC) Cuk converter.

Figure 9a shows the equivalent circuit when the switch is turned ON (conducting). Source voltage V_{in} charges parallel connected inductors L_1 and L_2 through the switch, diodes D_1 and D_3. Parallel connected inductors L_3 and L_4 supply power to load through diodes D_6 and D_8 and switch by the help of capacitor C_1 and C_2. During this mode, reversed biased diodes are diode D_2, D_4, D_5 and D_7. As inductors L_1 and L_2 are the same, an equal amount of current flows through them. Similarly, inductors L_3 and L_4 are the same; an equal amount of current flows through them. Figure 9b shows the current direction when the switch is turned OFF (not conducting). Parallel connected capacitors C_1 and C_2 are charged by source voltage V_{in}, inductors L_1 and L_2. Similarly, energy discharge by inductors L_3 and L_4 also charge the capacitors C_1 and C_2, and also provide power to load. During this mode, reversed biased diodes are diodes D_1, D_3, D_6 and D_8.

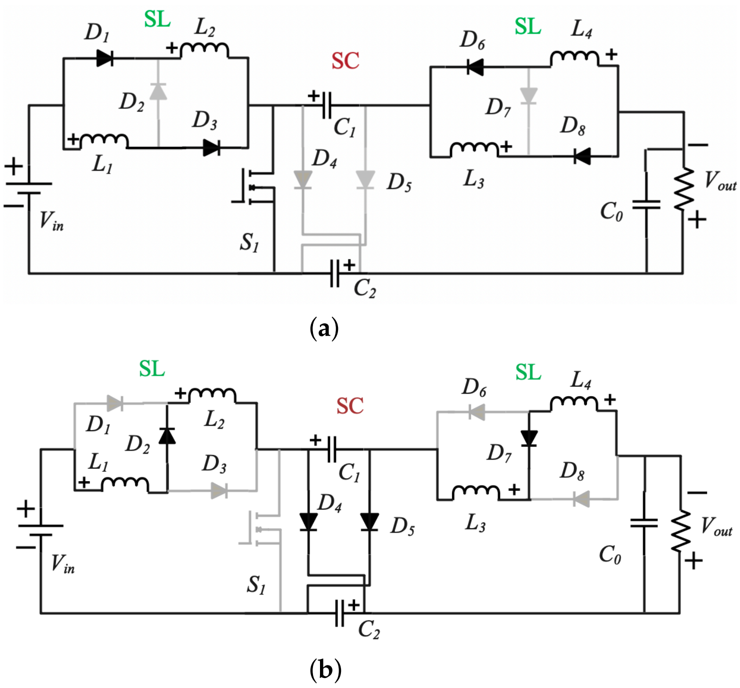

Figure 9. Topology 3: Operating mode of SLSC CUK converter (**a**) ON Mode (**b**) OFF Mode.

Design Analysis of Topology-3

When the switch S_1 is turned ON, the voltages for inductors are given as:

$$V_{L1} = V_{L2} = V_{in} \tag{37}$$

$$V_{L3} = V_{L4} = 2V_C - V_{out} \tag{38}$$

where, $V_C = V_{C1} = V_{C2}$. When switch S_1 is turned off the voltages for the inductors are given as:

$$V_{L1} = V_{L1} = \frac{V_{in} - V_C}{2} \tag{39}$$

$$V_{L3} = V_{L4} = \frac{V_C - V_{out}}{2} \tag{40}$$

Applying the volt-second method:

$$V_{in}D + (\frac{V_{in} - V_C}{2})(1 - D) = 0 \tag{41}$$

$$(\frac{2V_C - V_{out}}{2})D + (\frac{V_C - V_{out}}{2})(1 - D) = 0 \tag{42}$$

The voltage gain is given by,

$$G = \frac{V_{out}}{V_{in}} = \frac{I_{in}}{I_{out}} = \frac{(1 + 3D)}{(1 - D)} \tag{43}$$

The expression of voltage across switch, capacitor C_1 and C_2 and reverse voltage across diodes (D_1–D_8) are given in Table 3.

Table 3. Equations of voltages for type-3 SLSC CUK converter.

Parameters	Expression
Capacitors C_1 and C_2	$\frac{1+D}{1-D}V_{in}$
Switch S_1	$\frac{1+D}{1-D}V_{in}$
Diodes D_1, D_3, D_6 and D_8	$\frac{D}{1-D}V_{in}$
Diodes D_2 and D_7	V_{in}
Diodes D_4 and D_5	$\frac{1+D}{1-D}V_{in}$

5. Simulation Results and Analysis

The suggested three converters were simulated in the MATLAB Simulink environment to analyze their performance and characteristics. The values of various parameters used for the simulation of these converters are illustrated in Table 4. These converters were simulated using a PV system as an input power source. The PV system was attached with a converter using a coupling capacitor.

The results obtained from topology 1 are presented in Figure 10. Figure 10a depicts the current stress and voltage stress on MOSFET S_1. Figure 10b depicts the voltage stress on the SC's two diodes D_4 and D_5. Figure 10c depicts the current waveform of inductors L_1, L_2 and L_3. When MOSFET S_1 is turned ON, the three inductors are charged and discharged when MOSFET S_1 is turned OFF. Figure 10d depicts the input voltage and output voltage waveforms of the converter.

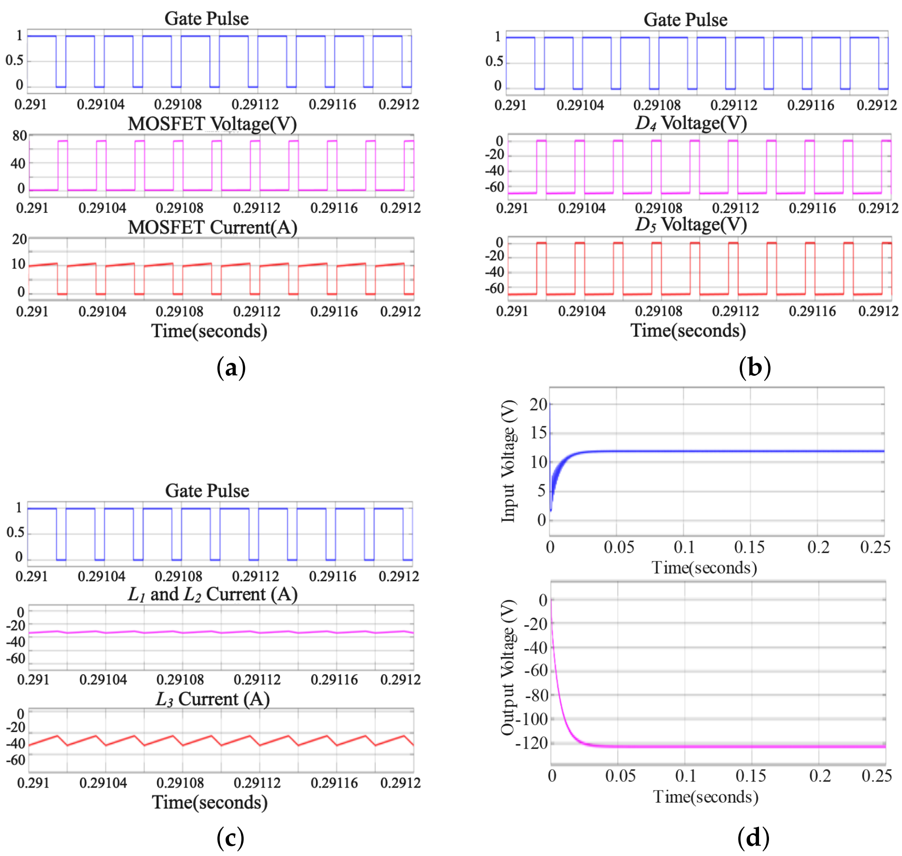

Figure 10. Simulation results of topology 1: (**a**) voltage and current of MOSFET (**b**) voltage across diodes (**c**) inductor's current (**d**) input and output voltage.

The results obtained from topology 2 are presented in Figure 11. Figure 11a depicts the current stress and voltage stress on MOSFET S_1. Figure 11b depicts the voltage stress on SC's two diodes D_1 and D_2. Figure 11c depicts the current waveform of inductors L_1, L_2 and L_3. When MOSFET S_1 is turned ON, the three inductors are charged and discharged when MOSFET S_1 is turned off. Figure 11d depicts the input voltage and output voltage waveforms of the converter.

The results obtained from topology 3 are presented in Figure 12. Figure 12a depicts the current stress and voltage stress on MOSFET S_1. Figure 12b depicts the voltage stress on the SC's two diodes D_4 and D_5. Figure 12c depicts the current waveform of inductors L_1, L_2, L_3 and L_4. When MOSFET S_1 is turned on, the four inductors are charged and discharged when MOSFET S_1 is turned off. Figure 12d depicts the input voltage and output voltage waveform of the converter.

Table 4. Parameter values used for simulation.

Parameters	Topology 1	Topology 2	Topology 3
Input Voltage (in Volts)	12	12	12
Switching Frequency (in kHz)	5	5	5
Inductor (in µH	600	600	600
Capacitor (in µF)	22	22	22
Load Resistance (in Ω)	190	75	210

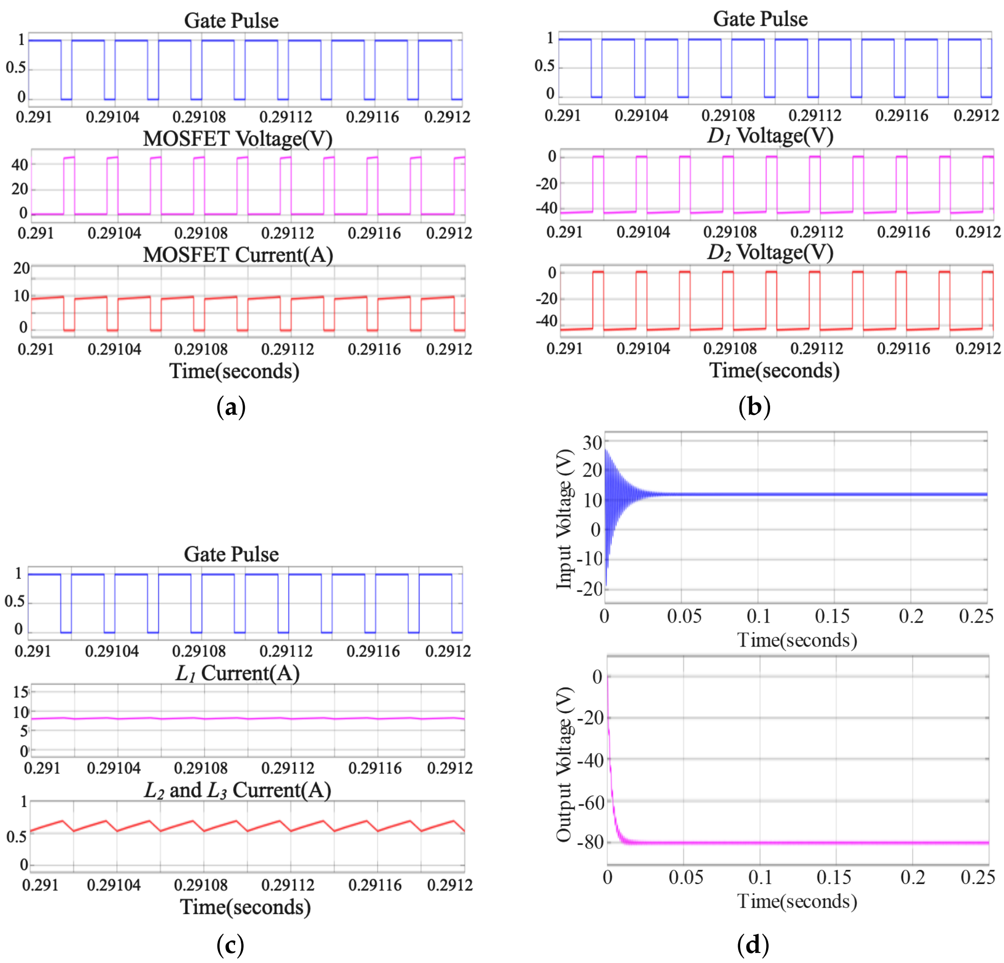

Figure 11. Simulation results of topology 2: (**a**) voltage and current of MOSFET (**b**) voltage across diodes (**c**) inductor's current (**d**) input and output voltage.

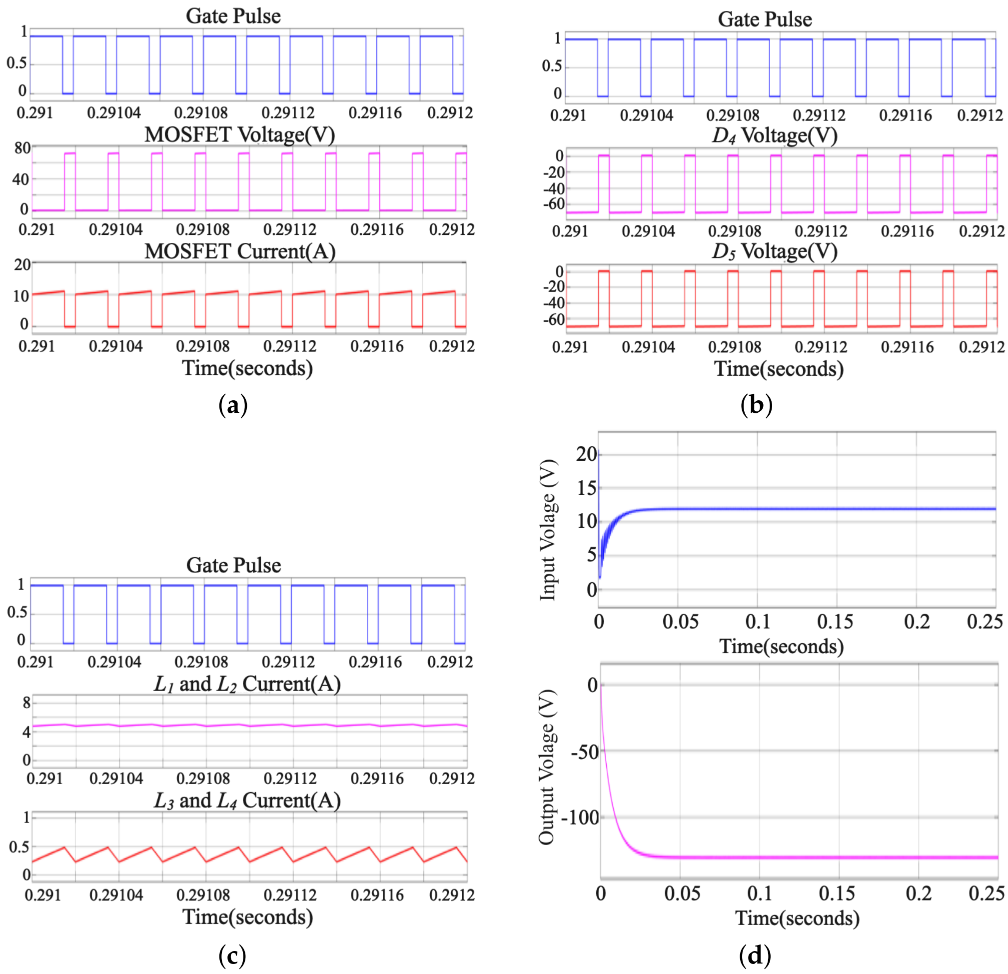

Figure 12. Simulation results of topology 3: (**a**) voltage and current of MOSFET (**b**) voltage across diodes (**c**) inductor's current (**d**) input and output voltage.

The number of components required for designing the three topologies of the SLSC Cuk converter and voltage gain formula is shown in Table 5. The comparative study of the voltage gain and normalized switch voltage stress for the three topologies of the SLSC Cuk converter with the conventional Cuk converter and boost converter is shown in Figures 13 and 14, respectively. It can be seen that the proposed converter topologies have higher gain than the conventional boost and Cuk converters. Out of the proposed three topologies, topology-3 has the highest gain, which can be seen in Figure 13. From Figure 14, it is concluded that conventional boost and Cuk converters have the highest normalised voltage stress compared to proposed converters.

Table 5. Comparison of Converters.

Parameter	Boost	Cuk	Topology 1	Topology 2	Topology 3
Diode	1	1	5	5	8
Capacitors	1	2	3	3	3
Inductors	1	2	3	3	4
Switch	1	1	1	1	1
Voltage Gain	$\frac{1}{1-D}V_{in}$	$\frac{D}{1-D}V_{in}$	$\frac{(1+D)^2}{1-D}V_{in}$	$\frac{1+3D}{(1+D)(1-D)}V_{in}$	$\frac{1+3D}{(1-D)}V_{in}$

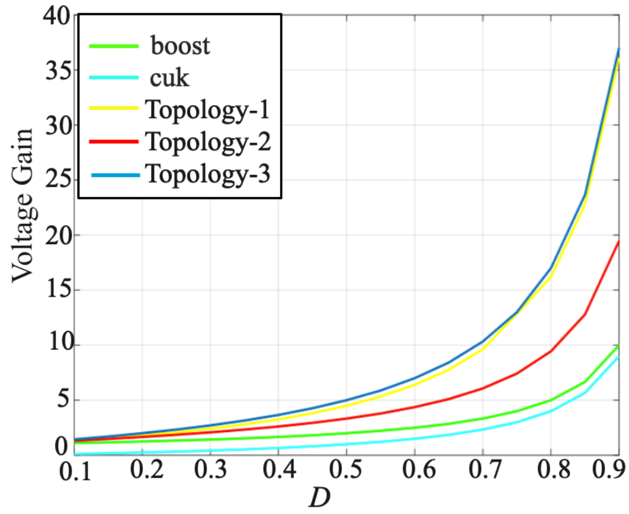

Figure 13. Comparison of converters in terms of voltage gain.

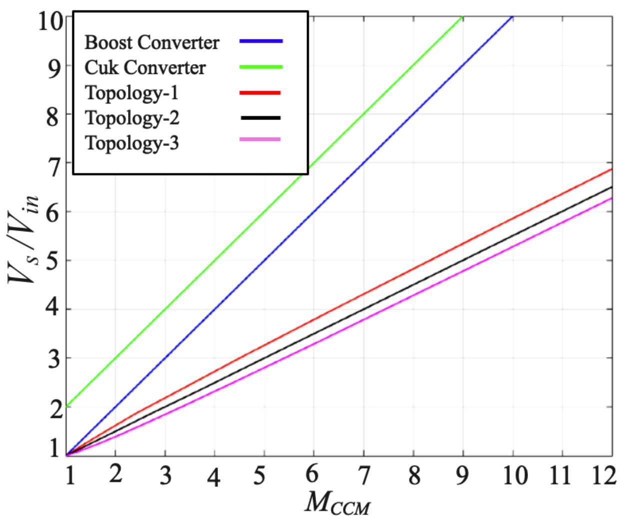

Figure 14. Comparison of converters in terms of normalized switch voltage stress.

6. Conclusions

In this study, the topologies of SLSC Cuk converters with low active switch strain and significant voltage gain were successfully designed. The continuous conduction mode operation of the converters was investigated. The suggested converters were controlled at a constant frequency using the PWM approach. The proposed converters were compared with traditional Cuk and boost converters. The suggested converters have several advantages, including low voltage stress and high voltage gain, which allow for selecting an active switch, a lesser voltage rating and low on-state resistance, continuous output and input currents, single switch operation, ease of design, and high efficiency. These converters were simulated with a 12 V PV source as an input of the converter on the MATLAB/Simulink platform. The current stress on the MOSFET switch of three topologies was 10 A. The voltage stress on the MOSFET switch of topology-1 and topology-3 was 78 V, while for topology-2, it was 46 V. Among these topologies, topology-2 provided the least voltage gain, while topology-3 provided the highest voltage gain. The hardware implementation can be considered for future study.

Author Contributions: Conceptualization, N.P., M.S.B., M.S. and D.K.D.; methodology, N.P. and F.A.; software, N.P., F.A., M.S. and D.K.D.; validation, N.P., M.S.B., I.B.M.T. and M.G.H.; formal analysis, N.P., M.S.B., F.A., I.B.M.T. and M.G.H.; investigation, N.P. and M.S.B.; resources, N.P. and M.S.B.; writing, N.P., F.A., M.S. and D.K.D.; writing, review and editing, M.S.B., I.B.M.T. and M.G.H.; visualization, M.S.B.; supervision, N.P. and M.S.B.; project administration, N.P., I.B.M.T. and M.G.H.; funding, I.B.M.T. and M.G.H. All authors have read and agreed to the published version of the manuscript.

Funding: This research was funded by the Taif University Researchers Supporting Project, grant number TURSP-2020/61.

Institutional Review Board Statement: Not applicable.

Informed Consent Statement: Not applicable.

Data Availability Statement: All data generated or analyzed during this study are included in this published article.

Acknowledgments: The authors would like to acknowledge the financial support received from the Taif University Researchers Supporting Project Number (TURSP-2020/61), Taif University, Taif, Saudi Arabia.

Conflicts of Interest: The authors declare no conflict of interest.

References

1. Khireddine, M.; Makhloufi, M.; Abdessemed, Y.; Boutarfa, A. Tracking power photovoltaic system with a fuzzy logic control strategy. In Proceedings of the 2014 6th International Conference on Computer Science and Information Technology (CSIT), Amman, Jordan, 26–27 March 2014; pp. 42–49.
2. Ranjana, M.S.B.; Reddy, N.S.; Kumar, R.K.P. Non-isolated dual output hybrid DC-DC multilevel converter for photovoltaic applications. In Proceedings of the 2014 2nd International Conference on Devices, Circuits and Systems (ICDCS), Coimbatore, India, 6–8 March 2014; pp. 1–6.
3. Musale, A.S.; Deshmukh, B.T. Three level DC-DC boost converter for high conversion ratio. In Proceedings of the 2016 International Conference on Electrical, Electronics, and Optimization Techniques (ICEEOT), Chennai, India, 3–5 March 2016; pp. 643–647.
4. Almalaq, Y.; Alateeq, A.; Matin, M. Silicon carbide DC-DC multilevel Cuk converter. In *Wide Bandgap Power Devices and Applications*; International Society for Optics and Photonics: Bellingham, DC, USA, 2016; Volume 9957, p. 99570I.
5. Li, W.; Lv, X.; Deng, Y.; Liu, J.; He, X. A review of non-isolated high step-up DC/DC converters in renewable energy applications. In Proceedings of the 2009 Twenty-Fourth Annual IEEE Applied Power Electronics Conference and Exposition, Washington, DC, USA, 15–19 February 2009; pp. 364–369.
6. Forouzesh, M.; Siwakoti, Y.P.; Gorji, S.A.; Blaabjerg, F.; Lehman, B. Step-up DC–DC converters: A comprehensive review of voltage-boosting techniques, topologies, and applications. *IEEE Trans. Power Electron.* **2017**, *32*, 9143–9178. [CrossRef]
7. Moradpour, R.; Ardi, H.; Tavakoli, A. Design and implementation of a new SEPIC-based high step-up DC/DC converter for renewable energy applications. *IEEE Trans. Ind. Electron.* **2017**, *65*, 1290–1297. [CrossRef]
8. Hsieh, Y.P.; Chen, J.F.; Liang, T.J.P.; Yang, L.S. Novel high step-up DC–DC converter with coupled-inductor and switched-capacitor techniques for a sustainable energy system. *IEEE Trans. Power Electron.* **2011**, *26*, 3481–3490. [CrossRef]
9. Choi, B.H.; Lee, S.W.; Thai, V.; Rim, C.T. A novel single-SiC-switch-based ZVZCS tapped boost converter. *IEEE Trans. Power Electron.* **2013**, *29*, 5181–5194. [CrossRef]
10. Salehi, S.M.; Dehghan, S.M.; Hasanzadeh, S. Interleaved-input series-output ultra-high voltage gain DC–DC converter. *IEEE Trans. Power Electron.* **2018**, *34*, 3397–3406. [CrossRef]
11. Ardi, H.; Ajami, A.; Sabahi, M. A novel high step-up DC–DC converter with continuous input current integrating coupled inductor for renewable energy applications. *IEEE Trans. Ind. Electron.* **2017**, *65*, 1306–1315. [CrossRef]
12. Heidari, M.; Farzanehfard, H.; Esteki, M. Single-Switch Single-Magnetic Core High Step-up Converter with Continuous Input Current and Reduced Voltage Stress for Photovoltaic Applications. In Proceedings of the 2019 10th International Power Electronics, Drive Systems and Technologies Conference (PEDSTC), Shiraz, Iran, 12–14 February 2019; pp. 695–700.
13. Abbasi, M.; Babaei, E.; Tousi, B. New family of non-isolated step-up/down and step-up switched-capacitor-based DC–DC converters. *IET Power Electron.* **2019**, *12*, 1706–1720. [CrossRef]
14. Premkumar, M.; Kumar, C.; Anbarasan, A.; Sowmya, R. A novel non-isolated high step-up DC–DC boost converter using single switch for renewable energy systems. *Electr. Eng.* **2020**, *102*, 811–829. [CrossRef]
15. Karimian, F.; Nahavandi, A. Design and analysis of a new structure of non-isolated DC–DC cuk–boost converter with high voltage gain. *IET Power Electron.* **2019**, *12*, 530–540. [CrossRef]
16. Chakraborty, S.; Verma, S.; Salgotra, A.; Elavarasan, R.M.; Elangovan, D.; Mihet-Popa, L. Solar-Based DG Allocation Using Harris Hawks Optimization While Considering Practical Aspects. *Energies* **2021**, *14*, 5206. [CrossRef]

17. Mahar, A.M.; Shaikh, P.H.; Mahar, A.R.; Memon, Z.A.; Khatri, S.A.; Shah, S.F. Simulation of efficient non-isolated DC-DC boost converter topology for photovoltaic application. *AIP Conf. Proc.* **2019**, *2119*, 020019.
18. Saravanan, S.; Babu, N.R. Analysis and implementation of high step-up DC-DC converter for PV based grid application. *Appl. Energy* **2017**, *190*, 64–72. [CrossRef]
19. Libra, M.; Petrík, T.; Poulek, V.; Tyukhov, I.I.; Kouřím, P. Changes in the Efficiency of Photovoltaic Energy Conversion in Temperature Range with Extreme Limits. *IEEE J. Photovoltaics* **2021**, *11*, 1479–1484. [CrossRef]
20. Poulek, V.; Šafránková, J.; Černá, L.; Libra, M.; Beránek, V.; Finsterle, T.; Hrzina, P. PV panel and PV inverter damages caused by combination of edge delamination, water penetration, and high string voltage in moderate climate. *IEEE J. Photovoltaics* **2021**, *11*, 561–565. [CrossRef]
21. Shemelin, V.; Matuska, T. Detailed modeling of flat plate solar collector with vacuum glazing. *Int. J. Photoenergy* **2017**, *2017*, 1587592. [CrossRef]
22. Priyadarshi, N.; Padmanaban, S.; Maroti, P.K.; Sharma, A. An extensive practical investigation of FPSO-based MPPT for grid integrated PV system under variable operating conditions with anti-islanding protection. *IEEE Syst. J.* **2018**, *13*, 1861–1871. [CrossRef]
23. Priyadarshi, N.; Padmanaban, S.; Bhaskar, M.S.; Blaabjerg, F.; Sharma, A. A fuzzy SVPWM based inverter control realization of grid integrated PV-wind system with FPSO MPPT algorithm for a grid-connected PV/wind power generation system: Hardware implementation. *Power Appl.* **2018**, *12*, 962–971.
24. Priyadarshi, N.; Padmanaban, S.; Holm-Nielsen, J.B.; Blaabjerg, F.; Bhaskar, M.S. An experimental estimation of hybrid ANFIS–PSO-based MPPT for PV grid integration under fluctuating sun irradiance. *IEEE Syst. J.* **2019**, *14*, 1218–1229. [CrossRef]
25. Priyadarshi, N.; Padmanaban, S.; Bhaskar, M.S.; Blaabjerg, F.; Holm-Nielsen, J.B.; Azam, F.; Sharma, A.K. A hybrid photovoltaic-fuel cell-based single-stage grid integration with Lyapunov control scheme. *IEEE Syst. J.* **2019**, *14*, 3334–3342. [CrossRef]
26. Priyadarshi, N.; Bhaskar, M.S.; Padmanaban, S.; Blaabjerg, F.; Azam, F. New CUK–SEPIC converter based photovoltaic power system with hybrid GSA–PSO algorithm employing MPPT for water pumping applications. *IET Power Electron.* **2020**, *13*, 2824–2830. [CrossRef]
27. Singh, M. *Power Electronics*; Tata McGraw-Hill Education: New York, NY, USA, 2008.
28. Chung, H.H.; Tse, K.; Hui, S.R.; Mok, C.; Ho, M. A novel maximum power point tracking technique for solar panels using a SEPIC or Cuk converter. *IEEE Trans. Power Electron.* **2003**, *18*, 717–724. [CrossRef]
29. Zhu, M.; Luo, F.L. Enhanced Self-Lift Ck Converter for Negative-to-Positive Voltage Conversion. *IEEE Trans. Power Electron.* **2010**, *25*, 2227–2233. [CrossRef]
30. Su-Won, L.; Lee, S.; Chil-Hwan, J. A New High Efficient Bi-directional DC/DC Converter in the Dual Voltage System. *J. Electr. Eng. Technol.* **2006**, *1*, 343–350.
31. Chen, Z. PI and sliding mode control of a Cuk converter. *IEEE Trans. Power Electron.* **2012**, *27*, 3695–3703. [CrossRef]